Faraday Discussions

Cite this: *Faraday Discuss.*, 2023, **241**, 394

PAPER

View Article Online
View Journal | View Issue

What stress components drive mechanochemistry? A study of ZDDP tribofilm formation†

Lu Fang,[a] Spyridon Korres,[b] William A. Lamberti,[b] Martin N. Webster[a] and Robert W. Carpick*[a]

Received 4th June 2022, Accepted 26th July 2022

DOI: 10.1039/d2fd00123c

Zinc dialkyldithiophosphate (ZDDP), the most widely used antiwear additive in engine oils, has been extensively studied over the last few decades to help understand the origin of its effectiveness. Glassy phosphate-based tribofilms, approximately 100 nm thick, are often formed on surfaces sliding in ZDDP-containing oils, which help to prevent or reduce wear. Recent studies reveal that a combination of applied shear and compressive stresses drive mechanochemical reactions that promote tribofilm growth, and that growth is further accelerated by increased temperature. While recent work has shown that compressive stress alone is insufficient to form tribofilms, the individual effects of the shear stress and compressive stress are not fully understood. Here, shear and compressive stresses are studied separately by using different ratios of high-viscosity, high-traction fluids for testing. This allows the areal mean compressive and shear stresses in the fluid when confined at a loaded sliding interface, to be independently controlled while driving tribofilm growth, which is a system we refer to as a stress-controlled mechanochemical reactor. Tribofilms derived from a secondary ZDDP were generated using a tungsten carbide/tungsten carbide ball-on-disk contact in the full elastohydrodynamic lubrication (EHL) regime using a mini-traction machine (MTM), meaning that solid–solid contact is avoided. The MTM was equipped with a spacer layer imaging (SLIM) capability, permitting *in situ* measurement of the tribofilm thickness during its growth. The well-separated sliding surfaces generated by the high-viscosity fluids confirm that solid–solid contact is not required for tribofilm formation. Under these full fluid film EHL conditions, shear stress and temperature promote tribofilm growth in accordance with stress-augmented thermal activation. In contrast, under constant shear stress and temperature, compressive stress has the opposite effect, inhibiting tribofilm growth. Using the extended Eyring model for shear- and hydrostatic pressure-affected reaction kinetics, an activation energy of 0.54 ± 0.04 eV is found, consistent with prior studies of ZDDPs. The activation volume for shear stress is found

---

[a] *Department of Mechanical Engineering & Applied Mechanics, University of Pennsylvania, Philadelphia, Pennsylvania 19104, USA. E-mail: carpick@seas.upenn.edu*

[b] *ExxonMobil Technology and Engineering Company, Annandale, NJ, 08801, USA*

† Electronic supplementary information (ESI) available. See https://doi.org/10.1039/d2fd00123c

to be 0.18 ± 0.06 nm^3, while that for the compressive stress component is much smaller, at 0.010 ± 0.004 nm^3. This not only confirms prior work supporting that shear stress drives tribofilm growth, but demonstrates and quantifies how compressive stress inhibits growth, consistent with the rate-limiting step in tribofilm growth involving a bond-breaking reaction. Implications of these findings are discussed.

1. Introduction

Lubricants are used to improve energy efficiency and reduce material damage by minimizing friction and preventing wear within sliding and rolling contacts. Most modern lubricants contain antiwear additives to protect the rolling and sliding components from severe wear under boundary and mixed lubrication regimes (*i.e.*, the lubricant film thickness is not enough to separate the two surfaces). Zinc dialkyldithiophosphates (ZDDPs), initially developed as corrosion and oxidation inhibitors in 1941,[1] are now the most common family of antiwear additives. The antiwear properties of ZDDPs were not discovered until 1955,[2] but due in part to the antiwear performance and cost-effectiveness are used in almost all commercially available engine oils.[3] The general molecular structure is shown in Fig. 1.[3]

The lubrication condition in sliding or rolling lubricated contacts depends directly on the thickness of the lubricant confined between the surfaces. This thickness increases with increasing entrainment speed (mean speed of the two surfaces), increasing lubricant viscosity, and decreasing applied pressure, resulting in a transition from direct solid–solid contact (the boundary regime) to a full fluid film between the surfaces (the hydrodynamic regime or, in the case of conformal contacts under high-load conditions, the elastohydrodynamic regime), with the mixed regime in between.[4] Under mixed and boundary lubrication conditions, ZDDPs decompose and form a protective surface-bound layer, known as a tribofilm, at locations where the surfaces experience sliding contact. The tribofilm prevents severe wear of the underlying substrate, particularly for ferrous-based materials, including steel, but also for other materials, such as silicon,[5] metals or metal alloys,[6–9] ceramics,[10–12] and diamond-like carbon (DLC) coatings.[13,14] Many classes of additives form tribofilms, however, due to the widespread use of ZDDPs and their crucial importance for wear protection, most studies have focused on ZDDP-derived tribofilms. The formation, composition, and structure of ZDDP-derived tribofilms have been studied for decades.[3] ZDDPs undergo a series of chemical reactions to initially form isolated pad-like tribofilms on the substrate. The isolated pads then grow together to form a thin, rough, and patchy iron and zinc phosphate-containing glassy tribofilm, which protects the underlying surfaces from wear.[15] Studies of these tribofilms have revealed that

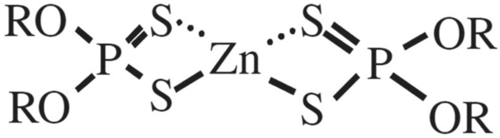

Fig. 1 ZDDP molecular structure. Types of ZDDPs are differentiated by their radical groups (R-group), which are often primary alkyls, secondary alkyls, or aryl groups.[3]

the mechanical properties and structure are varied throughout the tribofilm, particularly with a substantial change in composition with depth. One earlier study by Bird and Galvin found that the tribofilms they studied consisted of polyphosphate in the uppermost layer, which gradually changed to orthophosphate and pyrophosphate near the substrate.[16] A thin sulfur-rich layer exists beneath this thick phosphate tribofilm, which may assist in bonding the tribofilm to the substrate.[6,17] ZDDP tribofilms exhibit self-limiting tribofilm growth, which results in tribofilms that are typically 50–100 nm thick.[18]

Although ZDDP-derived tribofilms have been studied substantively, the mechanisms driving their growth and properties are still not well understood. Investigating the driving forces that trigger the initiation and growth of the tribofilm is the key to unlocking a better understanding of ZDDP-tribofilm formation. Establishing a better understanding of these processes will allow development of optimized antiwear technologies in a broadening range of conditions. In particular, to protect vehicle emission systems, the levels of metals, P, and S are limited in fully formulated engine oils.[19] Furthermore, changes in vehicle drivetrain configurations, including the increasing use of electric vehicles (EVs), hybrid technologies, and alternate fuels, result in changes to the demands on, and the operating environment for, antiwear additives.[20,21] While studies have focused on ZDDPs, the understanding of these mechanisms is potentially relevant to a broad range of antiwear, extreme pressure, and friction-modifier additives. For example, the self-limiting growth of tribofilms derived from solid nanoparticles that provide antiwear performance has been reported recently.[22–25] Ultimately, knowledge of tribofilm initiation and growth will allow optimization of current additives in different applications and environments, and will help guide new additive technologies.

Recent attention has turned to the study of how mechanochemical mechanisms play a role in ZDDP-tribofilm formation at the nano-,[5,26] micro-,[9,27] and macroscale.[12,28] Several recent studies have focused on the specific role that applied stress has on tribofilm generation.[5,9,12,26–28] Experimental studies include the use of *in situ* bench-scale testing methods, such as single-asperity atomic force microscopy (AFM) methods and mini-traction machines with spacer-layer imaging (MTM-SLIM). Gosvami *et al.* were the first to explore the mechanochemical response of ZDDP by using AFM.[5] In their study, they used a sharp amorphous carbon-coated AFM tip scanning over a nanoscale area on a pure iron substrate (with a native oxide) under different applied normal loads and temperatures in a commercial-grade synthetic hydrocarbon oil containing a standard commercial ZDDP package involving primary and secondary ZDDP molecules. The morphology of the rubbed area was periodically monitored using the AFM imaging mode, allowing tribofilm growth to be quantified over time. Compressive stress (based on the mean value estimated from Hertzian mechanics applied to the tip–substrate contact) and temperature were found to be the main driving forces of the ZDDP decomposition and antiwear tribofilm formation, although the authors noted that they could not discount the possibility that shear stress – intrinsic to the sliding contact and directly correlated with the applied compressive stress – was driving tribofilm growth. The tribofilm growth rate followed the stress-augmented thermal activation (SATA) model.[29] Using a secondary ZDDP molecule, and then an ashless DDP, another single-asperity study by Dorgham *et al.* (Si tip, steel substrate) also showed that the reaction kinetics followed the SATA model.[26]

One way in which stress may play a role is by inducing different levels of cross-linking within a polyphosphate tribofilm. According to molecular dynamics simulations by Mosey *et al.* of a simplified phosphorous-based tribofilm precursor molecule, cross-linking of a polyphosphate tribofilm increases strongly with compressive stress once the stress exceeds a threshold value of 5 GPa.[30–33] This may explain why ZDDP-derived tribofilms do not form well on softer Al-based alloys, since their low hardness compared to steel (750–920 HV *vs.* 170–190 HV[8]) will prevent contact stresses from reaching the threshold value. Consistent with this idea, Gosvami *et al.* observed, using the AFM technique, that initially no ZDDP-derived tribofilm forms, and substantial plastic deformation of the Al occurs.[9] After sufficient plastic deformation, the tribofilm forms, attributed to work hardening of the Al and thus higher compressive stress of the contact, leading to stress-induced tribofilm formation. There could also be mechanochemically-activated processes that play a role. For example, Loehlé and Righi used *ab initio* molecular dynamics (AIMD) simulations to study a simple organophosphorous molecule, trimethylphosphite (TMPi), that is known to form tribofilms in experiments.[34] The AIMD results showed that TMPi, when compressed between sliding iron surfaces, reacts with the iron surfaces to form iron phosphide, and that the reaction rate is faster than that expected on a free surface. The difference is attributed to force-induced confinement. Collectively, these studies show that compressive stress can influence the growth rate as well as the chemical composition and the mechanical properties of the tribofilm.

Recently, Zhang and Spikes used MTM-SLIM in an innovative way to provide even more evidence that the growth kinetics of tribofilm formation followed the SATA model.[12] These experiments were conducted under full film elastohydrodynamic lubrication (EHL) conditions and demonstrated that surface-bound tribofilms can be formed in the absence of direct surface contact. The stress driving the growth comes from the compressive and shear stresses in the fluid acting on the precursor molecules, leading to tribofilm growth at the fluid–solid interface, instead of from the solid surfaces that confine the tribofilm precursor molecules and compress and shear them. The experiments were conducted under mixed rolling–sliding conditions using a high-EHL-traction fluid in order to attain high shear stresses. The work revealed that shear stress is required to drive tribofilm generation and subsequent growth. In a subsequent study, using the same technique, Spikes and coworkers showed that the ZDDP-derived tribofilm growth rate was found to be independent of ZDDP concentration in the solution, indicating that the reaction follows zero-order kinetics.[28]

A limitation of all of these previous studies is that it was not possible to independently control and vary the compressive stress and shear stress. In both sets of AFM experiments, the initial compressive stress (in the absence of the tribofilm) was used as the characteristic stress for model fitting. However, the elastic modulus of ZDDP tribofilms is much lower than that of the ferrous-based substrate (15–90 GPa (ref. 35) *vs.* 211 GPa (ref. 5)). Therefore, both the compressive and shear stress change during the experiments as the tribofilm grows under the AFM probe; in fact, a reduction in these stresses as the tribofilm grows potentially explains the saturation of the tribofilm thickness. In addition, wear of the AFM probe can alter the compressive and shear stresses in the contact. In Dorgham *et al.*'s study,[26] the estimated radius of silicon AFM probes increased from an initial value of 15 nm to approximately 80 nm under an applied force of 150 nN. Even under no applied force (*i.e.*, only a small adhesive force acts), the probe radius increased to approximately 50 nm. Thus, the true stress state varies significantly over the course of the experiment, which is likely to impact tribofilm growth rates, although the rate of change of the tip radius reduces significantly as the experiment proceeds. Regardless, the lack of control of tip size, and lack of ability to independently vary the shear and compressive stresses, are key limitations of this approach.

In the MTM studies,[12,28] the applied shear stress was controlled by altering the applied normal load. The shear stress generated within the EHL contact is determined by the high compression and shear properties of the lubricant used. For a single fluid, the shear stress generated in the contact region varies with temperature and compressive stress, preventing the independent variation of all three and thus making it challenging to determine their effects independently.

The goal of the present work is to determine the independent effects of compressive stress, shear stress, and temperature on tribofilm-formation kinetics. The experiments were performed using the MTM-SLIM methodology previously developed by Zhang and Spikes,[12] but modified to permit independent variation of shear and compressive stresses at chosen temperatures. Specifically, we used different combinations of lubricant basestocks to produce a series of blends with different EHL-traction properties. These all contained the same amount of ZDDP, thus allowing us to independently vary the shear stress, compressive stress, and temperature without any alteration of the chemically-active species in the lubricant. To effectively eliminate the likelihood of direct surface contact, the fluid blends were chosen to have sufficiently high viscosity, thus sufficiently thick EHL films were generated, allowing independent study of the stress components driving ZDDP-derived tribofilm formation.

2. Materials and test methods

2.1 Lubricant samples

A total of 9 different lubricant blends were used in the study, each containing 99 wt% of basestocks and 1 wt% ZDDP. The basestocks contain different combinations of a high-EHL-traction fluid, polyisobutene (PIB) and a low-EHL-traction fluid, polyalphaolefin, with a kinematic viscosity of 40 cSt at 100 °C (PAO40). The ZDDP was a commercially available secondary-type ZDDP. The detailed information is provided in the ESI, Table S1.†

2.2 Test methods

The PCS Instruments MTM-SLIM (London, UK) was used to generate both traction data *vs.* time and concurrent periodic *in situ* tribofilm thickness measurements throughout the duration of the test, as well as to determine traction curves. In addition, the final end-of-test film profile was measured using a 2D surface profilometer, Tencor™ P-7 (Milpitas, CA) to verify the accuracy of the SLIM measurements. The root-mean-square roughness of the ball and the disk was measured using a Zygo NewView™ 6300 (Middlefield, CT) white-light interferometer. The central lubricant film thickness was measured using a PCS EHD2 rig

(London, UK). A TESCAN S8000X (Kohoutovic, Czech Republic) focused ion beam-scanning electron microscope (FIB-SEM) equipped with a time-of-flight secondary ion mass spectrometer (ToF-SIMS) was used to study the chemical composition of the tribofilms.

3. Results and discussion

The fluid blends used in this study contained different combinations of lubricant basestocks of a high-traction base fluid (polyisobutylene, PIB), and a low-traction base fluid (polyalphaolefin, PAO). At a given compressive stress, P, and temperature, T, the shear stress, τ, will depend on the PAO/PIB ratio, thus allowing independent control of the compressive and shear stresses at each temperature by using different fluid mixtures. We call this the "stress-controlled mechanochemical reactor". The full information for each blend is given in the ESI, Table S1.† The compressive stress reported for each combination of lubricant composition and temperature is the calculated maximum Hertzian pressure, and the shear stress is obtained from the multiplication of the compressive stress and the traction coefficients measured based on the traction curves in Fig. S3 and S4.† The experiments were conducted with a tungsten carbide ball and disk to perform experiments up to high stresses, while avoiding plastic deformation. During the MTM experiment, the shear stress over time stays stable as shown in Fig. S8.† The properties of the specimens are provided in Table S2.† The specific lubricant film thickness, which indicates whether the surfaces are sufficiently separated to avoid solid–solid contact, is given by the ratio of the central lubricant film thickness (estimated using the well-established EHL theory[4] to be at least 116.5 nm for all experiments) and the composite roughness of the solid surfaces (measured using white light interferometry to be 5.4 nm) (eqn (S3)†).[4] This corresponds to a specific lubricant film thickness of 21.6 or greater, which indicates that there is, as desired, a large fluid separation between the ball and the disk. The growth rate of the ZDDP tribofilm was extracted from the initial 30 minutes of the 6 hour experiments, since tribofilm saturation was observed to begin at that point or later. An initial nucleation period, observed to last approximately 10 minutes, was excluded from the analysis, as shown in Fig. S10–S12.†

The morphology of the tungsten carbide (WC) disk underlying the ZDDP tribofilm was observed after tribofilm removal with EDTA. White-light interferometry (WLI) measurements with a vertical resolution better than 1 nm reveal no observable wear of the WC; a representative example is shown in Fig. 2. This shows that consumption of substrate material is not needed to grow the tribofilm. This contrasts with the hard and soft acid–base (HSAB) reaction model for ZDDP tribofilm growth, which posits that substantial generation of wear particles is required to form ZDDP tribofilms.[36] In the case of ferrous surfaces, the acid–base reaction involves the exchange of the softer Lewis acid, Zn^{2+} from ZDDP molecules, with the harder Lewis acid, Fe^{3+} from substrate-derived iron oxide wear particles, which prefers to interact with phosphates from the ZDDP, which are harder Lewis bases. While such an ion exchange will modify the tribofilm composition and properties, the results here show that robust ZDDP tribofilms can be formed without Fe or other significant wear-debris generation.

Time-of-flight secondary ion mass spectrometry (ToF-SIMS) was used to investigate the composition of the ZDDP-derived tribofilms on the WC disk. The

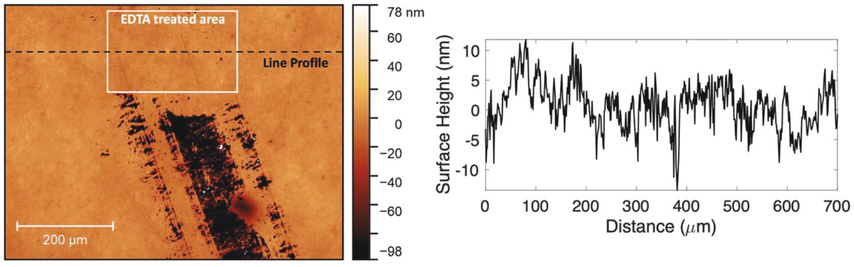

(a)

(b)

Fig. 2 (a) White light interferometry (WLI) image of the running track on the WC disk after tribofilm removal with EDTA. The negative height measurement in the tribofilm area is an artifact due to the internal reflections within the transparent ZDDP tribofilm, as reported previously.[37] (b) Line profile of the EDTA-treated area of the WC disk, showing no observable wear.

analytical conditions for SIMS analysis are shown in the ESI.† Stevie *et al.* demonstrated the ToF-SIMS instrument setup in ref. 38. The positive and negative mass-spectra comparison between the outer layer (approximately 1.7 nm) of the WC disk surface, which has been exposed to the ZDDP-containing blend during the MTM experiment, and the outer layer of the tribofilm are shown in Fig. 3(a)

(a) Positive Mass Spectra

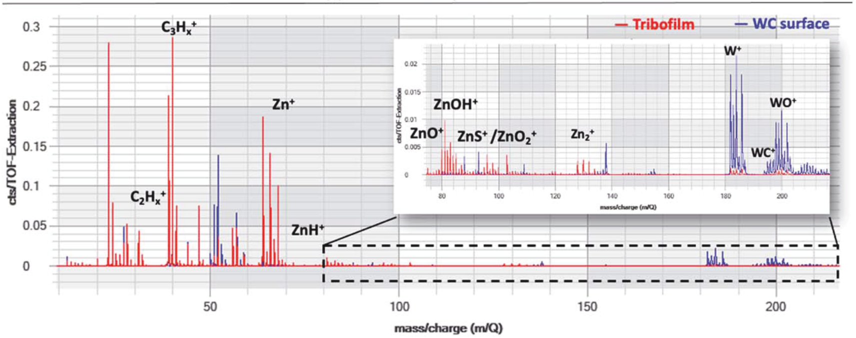

(b) Negative Mass Spectra

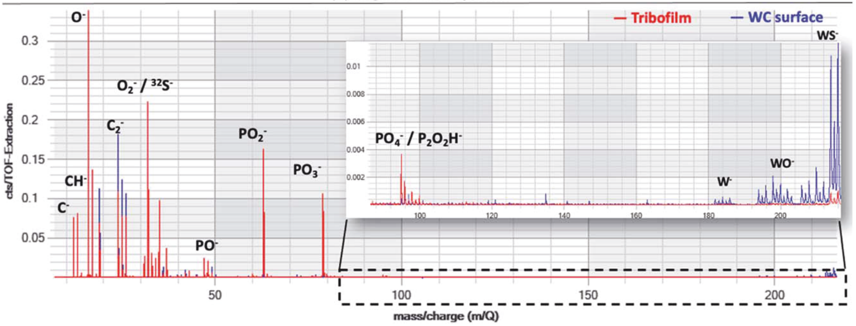

Fig. 3 The (a) positive and (b) negative ion spectra comparison between the top layer (approximately 1.7 nm) of the tribofilm and WC surface.

and (b), respectively. In the tribofilm area, there are several peaks attributed to hydrocarbon fragments ($C_2H_x^+$ and $C_3H_x^+$), and zinc-containing species (Zn^+, ZnO^+, $ZnOH^+$, ZnS^+ or ZnO_2^+, and Zn_2^+), while tungsten-containing peaks (W^+, WC^+, and WO^+) are absent, as expected. In addition, a large amount of O^- and a series of peaks attributed to phosphates (PO^-, PO_2^-, PO_3^-, and $P_2O_2H^-$) were found. Outside of the running track, a significant amount of WS^- was observed. This indicates that ZDDP reacts with the WC surface by either physisorption that is strong enough to remain after rinsing the sample, or forming a layer rich in W and S (*e.g.*, tungsten sulfide, sulfate or mixed sulfides/oxides).

Fig. 4(a) is the ion-induced secondary electron image (iSEI) of a 400 × 400 μm^2 area, where the bright vertical stripe is the tribofilm that has grown in the running track, and the dark area is the WC substrate outside the running track. Corresponding secondary ion images of relevant elements were selected for ZDDP tribofilm chemical investigation. The element distribution maps of Zn^+ and W^+ in Fig. 4(b) and (c) indicate that the tribofilm is mainly Zn^+ and lacks W^+. Only a small amount of W^+ is incorporated into the tribofilm, therefore, the gradient in the W^+ signal seen near the bottom of the tribofilm is most likely attributed to the ion beam mixing effect, where the primary ions can drive surface atoms ahead of

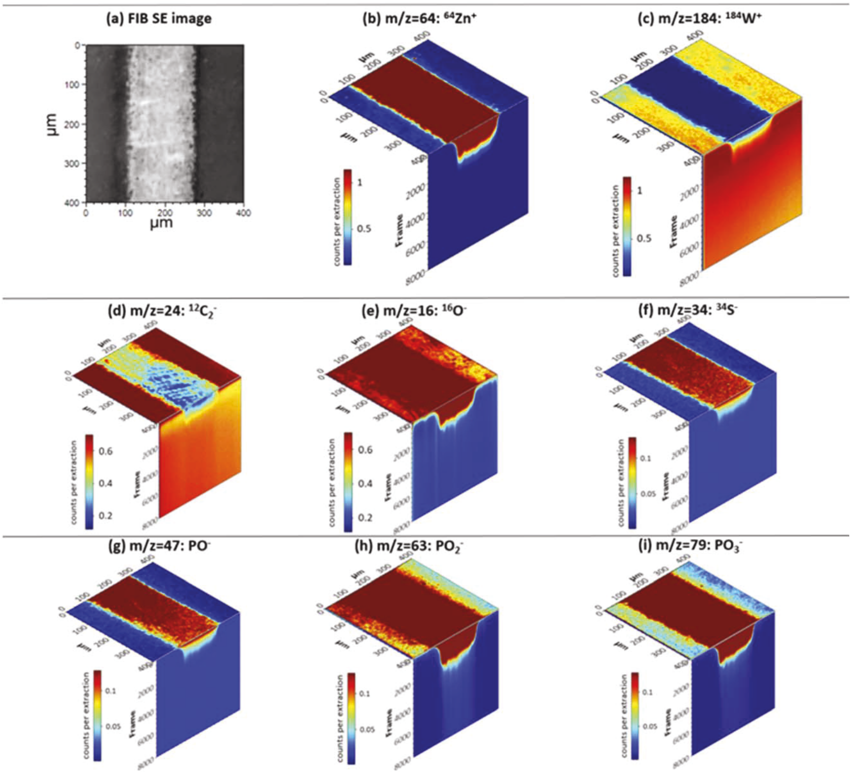

Fig. 4 (a) Ion-induced secondary electron image of the analyzed area, where the white region is the ZDDP-induced tribofilm, and the dark area is WC substrate. (b) and (c) are the 3D view of the $^{64}Zn^+$ and $^{184}W^+$ element distribution in the analyzed area respectively. The element distributions of (d) $^{12}C_2^-$, (e) $^{16}O^-$, (f) $^{34}S^-$, (g) PO^-, (h) PO_2^-, (i) PO_3^- in the analyzed area.

the sputtering interface into the sample.[39] Interface roughening can also arise as sputtering proceeds, resulting in a loss of depth resolution during analysis. This result is consistent with the WLI result of Fig. 2, indicating that no wear of the WC substrate is involved in tribofilm growth. Nonetheless, some diffusional mixing at the original surface cannot be ruled out from this analysis alone. The intensity of $^{12}C_2^-$, shown in Fig. 4(d), gets higher as the milling approaches the WC surface. Since sulfur is difficult to identify as the difference in the mass number of $^{16}O_2^-$ and $^{32}S^-$ is subtle, the distribution of results with a mass-to-charge ratio of 32 can be a combination effect from both $^{16}O_2^-$ and $^{32}S^-$. A second isotope of sulfur, $^{34}S^-$, was also chosen for analysis, and Fig. 4(f) shows that sulfur is mostly observed in the top layer of the tribofilm. The element distribution maps of Fig. 4(g)–(i) show that the tribofilm likely contains a significant amount of phosphate (PO^-, PO_2^-, PO_3^-). Therefore, the tribofilm is composed primarily of zinc and phosphate species, with enhanced S-content at the surface, consistent with the typical composition of ZDDP-derived tribofilms studied previously.[3,17,40–43]

3.1 Effect of compressive stress

In the first set of experiments, we varied the blend composition and the normal load to quantify the growth of tribofilms as a function of the compressive stress, with a fixed shear stress and temperature as shown in Table 1. This was done for two different pairs of temperature and shear stress values. The results show that with the temperature and shear stress held constant, increasing the compressive stress reduces the rate of tribofilm growth as shown in Fig. 5. This demonstrates for the first time that compressive stress inhibits ZDDP tribofilm growth.

3.2 Effect of shear stress

In the second set of experiments, we explored the independent effect of shear stress on growth. Another series of different lubricant blends were formulated as shown in Table 2. Two sets of experiments were performed at the same compressive stress of 2.5 GPa, but at two different temperatures, 100 °C and 140 °C.

Fig. 6 shows that the growth rate increases with applied shear stress, which confirms that the shear stress is a primary driving force for growing the tribofilms, as demonstrated by Zhang and Spikes.[12,28]

Table 1 Summary of blend information and contact stress

Experiment subset 1 ($T = 140$ °C; $\tau = 194 \pm 2$ MPa)		Experiment subset 2 ($T = 120$ °C; $\tau = 207 \pm 2$ MPa)	
Fluid composition	Compressive stress (GPa)	Fluid composition	Compressive stress (GPa)
89% PIB + 10% PAO	2.2	99% PIB	2
84% PIB + 15% PAO	2.3	89% PIB + 10% PAO	2.2
79% PIB + 20% PAO	2.4	84% PIB + 15% PAO	2.3
74% PIB + 25% PAO	2.5	79% PIB + 20% PAO	2.4

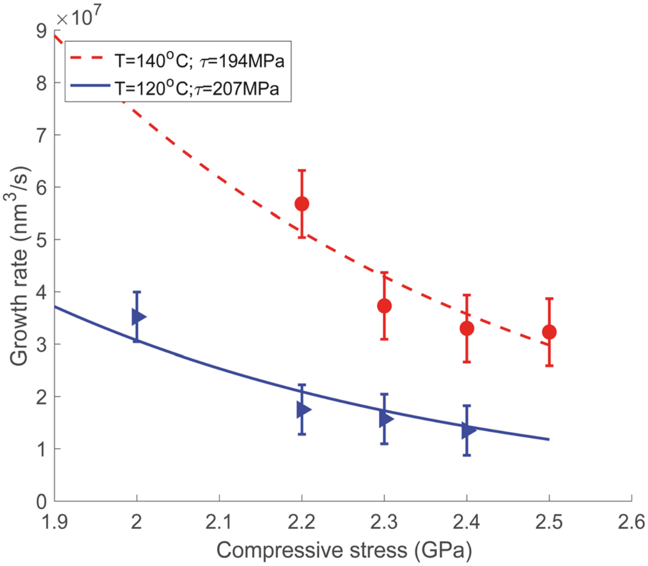

Fig. 5 Dependence of tribofilm growth rate on the compressive stress. The legend indicates the values of temperature and applied shear stress used. The red dotted line and the blue solid line are fits of the extended Eyring model (eqn (3)) at the respective temperatures and shear stresses.

Table 2 Summary of blend information and shear stresses for two sets of experiments

Experiment subset 1 ($T = 140$ °C; $P = 2.5$ GPa)		Experiment subset 2 ($T = 100$ °C; $P = 2.5$ GPa)	
Fluid composition	Shear stress (MPa)	Fluid composition	Shear stress (MPa)
99% PIB	260	99% PIB	279
89% PIB + 10% PAO	234	89% PIB + 10% PAO	258
84% PIB + 15% PAO	218	79% PIB + 20% PAO	233
79% PIB + 20% PAO	207	64% PIB + 35% PAO	205
74% PIB + 25% PAO	196		

3.3 Effect of temperature

In the third set of experiments, we studied the effect of temperature on tribofilm growth rate. Two subsets of experiments were performed, shown in Table 3, with the compressive stress the same for both, and two different target shear stresses used since shear stress affects film growth strongly. For each experiment subset, the target shear stress was approximately constant throughout the temperature range. To achieve the target shear stress, different blends were selected to run at each combination of temperature and pressure. Set 1 was run with a compressive stress of 2.5 GPa and a shear stress of approximately 233 MPa. The other set was run under the same compressive stress, but at a lower shear stress of 207 MPa.

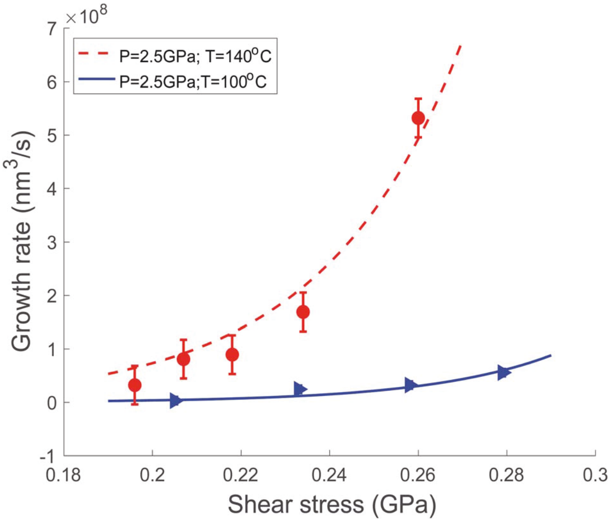

Fig. 6 Dependence of tribofilm growth rate on the shear stress. The legend indicates the values of temperature and applied compressive stress used. The red dotted line and the blue solid line are fits of the extended Eyring model (eqn (3)) at the respective temperatures and compressive stresses.

Table 3 Summary of blend information and applied temperature in Celsius for two sets of experiments

Experiment subset 1 ($P = 2.5$ GPa; $\tau = 233 \pm 2$ MPa)		Experiment subset 2 ($P = 2.5$ GPa; $\tau = 207 \pm 2$ MPa)	
Fluid composition	Temperature (°C)	Fluid composition	Temperature (°C)
89% PIB + 10% PAO	140	79% PIB + 20% PAO	140
84% PIB + 15% PAO	120	74% PIB + 25% PAO	120
79% PIB + 20% PAO	100	64% PIB + 35% PAO	100
74% PIB + 25% PAO	80	54% PIB + 45% PAO	60

The results shown in Fig. 7 illustrate that increasing the temperature also accelerates the tribofilm growth rate. Therefore, as seen consistently with all studies of ZDDP,[3,5,12,28] tribofilm formation is thermally driven.

3.4 Extended Eyring model

The SATA model, which describes how activated processes, including tribofilm growth, are affected by stress, derives from multiple sources.[29] One starting point is the model proposed by Bell,[44] which is now widely used as the basis for mechanochemistry and tribochemistry,[29] which proposed that the rate of force-assisted bond breakage can be determined by the following equation:

$$k = A\exp\left(-\frac{\Delta U_{\text{act}} - f\Delta x_{\text{act}}}{k_{\text{B}}T}\right) \tag{1}$$

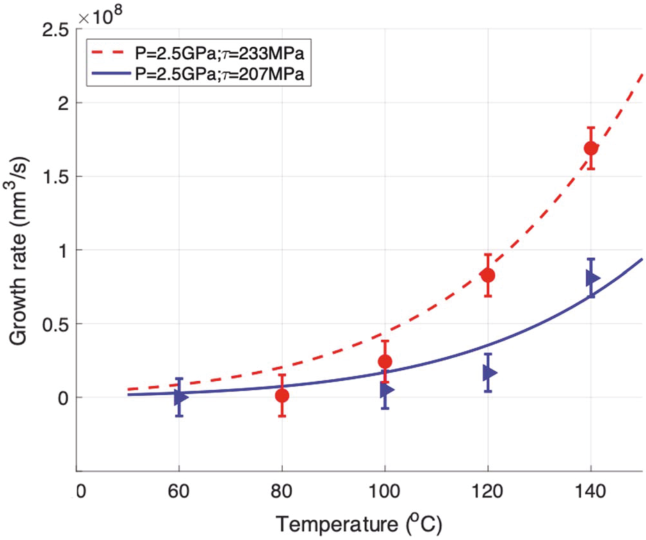

Fig. 7 Dependence of tribofilm growth rate on the temperature. The legend indicates the values of applied compressive stress and shear stress used. The red dotted line and the blue solid line are fits of the extended Eyring model (eqn (3)) at the respective temperatures and compressive stresses.

where k is the rate constant, A is a pre-exponential factor, ΔU_{act} is the activation energy, k_B is Boltzmann's constant, and T is temperature. The force, f, applied to the system assists the forward reaction rate if it drives the system along the reaction coordinate.[45] The reaction rate is also determined by the activation length, Δx_{act}, which is defined as the difference in linear size of the reacting species in the transition state *vs.* the initial state. To reduce the energy barrier, the work done on the system, $f\Delta x_{\text{act}}$, involves the component of the force along the direction of the chemical reaction process. If f is a driving force applied along the specific bond or on a molecule, the energy barrier will be reduced by $|f\Delta x|$. For example, a force that extends the length of a molecule will lower the activation barrier for a bond-breaking process. However, if f is an inhibitory force, the energy barrier will be increased, thus the work done to the system is negative, which is $-|f\Delta x|$. In practice, the applied force at the molecular level is complex to measure. However, it is feasible to estimate the applied stress during experiments, which corresponds to the average force applied per molecule assuming a uniform areal density of molecules. Thus, instead of activation length, one uses the activation volume. In this case, the rate constant is given by the following equation:[29]

$$k = A\exp\left(-\frac{\Delta U_{\text{act}} - \sigma\Delta V_{\text{act}}}{k_B T}\right) \tag{2}$$

where σ is the applied stress, and ΔV_{act} is the activation volume. ΔV_{act} is the difference in volume between the transition state (V_{TS}) and the initial equilibrium state of the reactant (V_R).[46] A positive activation volume indicates that the volume of the transition state is larger, which would be the case for a bond-breaking reaction. In contrast, a negative activation volume indicates the volume of the transition state is smaller, which indicates that the applied stress is helping with bond formation.

The importance of the hydrostatic and shear components of stress in driving activated processes was considered by Ward in 1971, who was studying the temperature and shear-rate dependence of polymer yields with applied tension and compression.[47] He introduced an extended form of the Eyring model that considered the effect of both the compressive stress and the shear stress as follows:

$$k = A\exp\left(-\frac{\Delta U_{\mathrm{act}} - \tau\Delta V_{\mathrm{act}} + P\Delta\Omega_{\mathrm{act}}}{k_{\mathrm{B}}T}\right) \tag{3}$$

where ΔV_{act} is the activation energy corresponding to the shear stress, τ, and $\Delta\Omega_{\mathrm{act}}$ is the activation energy corresponding to the compressive stress, P (the equation has been adapted from Ward to represent a growth rate, as opposed to a shear rate). With applied shear stress, a tension force can act on molecules that are constrained at their ends, which can promote bond breakage. If a bond-breaking reaction is the rate-limiting step in tribofilm growth, then shear stress is expected to increase the tribofilm formation rate and indeed the term $-\tau\Delta V_{\mathrm{act}}$ inside the exponential will do just that. On the other hand, compressive stress will inhibit bond stretching and breaking. Thus, again, if a bond-breaking reaction is the rate-limiting step in tribofilm growth, the activation barrier will increase. The term $P\Delta\Omega_{\mathrm{act}}$ inside the exponential will also have that effect, where a positive value of P is used for the case of applied compressive stress. Such bond-breaking interactions could involve cleavage of sulfur and zinc bonds, or those between sulfur and alkyl groups, and are discussed further below.

Since the tribofilm volume increases approximately linearly with time, it can be modeled as a zeroth-order reaction, which was confirmed in MTM experiments by Zhang *et al.*[28] Therefore, the growth rate of the tribofilm, Γ, can be modeled as the following:

$$\Gamma = \Gamma_0\exp\left(-\frac{\Delta U_{\mathrm{act}} - \tau\Delta V_{\mathrm{act}} + P\Delta\Omega_{\mathrm{act}}}{k_{\mathrm{B}}T}\right) \tag{4}$$

where Γ_0 is defined as:

$$\Gamma_0 = V_{\mathrm{m}}\nu \tag{5}$$

where V_{m} is the molar volume, assumed to be 1 nm^3 in the ZDDP tribofilm, and ν is the attempt frequency. We obtained high-quality fits by using the values of parameters in Table 4 to fit the data sets in Fig. 4–6.

The positive activation volumes found with two different components of stress indicate that a bond-breaking reaction is the rate-limiting step for tribofilm formation. The value of the activation energy estimated here is similar to ones found for ZDDP tribofilms grown on ferrous-based surfaces, which are between 0.58 to 1 eV, as measured by both AFM[5] and MTM[12,28] studies. This comparable value may indicate that any chemical reactivity differences between ferrous and WC-based surfaces for tribofilm growth are not dominant. Our energy barrier being on the lower end of the published range is consistent with our use of a secondary ZDDP; secondary ZDDPs grow tribofilms faster than primary ZDDPs and this may be due to a lower activation barrier, although the faster growth may

Table 4 The prefactor, Γ_0, activation energy, ΔU_{act}, activation volume for shear stress, ΔV_{act}, and activation volume for compressive stress, $\Delta \Omega_{\text{act}}$, obtained from fittings of six different experiments

	Experiment	Γ_0	ΔU_{act}	ΔV_{act}	$\Delta \Omega_{\text{act}}$
Compressive stress	Subset 1	2.16×10^{13}	0.54 eV	0.18 nm^3	0.01 nm^3
	Subset 2	1.10×10^{13}			
Shear stress	Subset 1	4.40×10^{13}			
	Subset 2	1.00×10^{13}			
Temperature	Subset 1	3.45×10^{13}			
	Subset 2	3.31×10^{13}			

also result from different attempt frequencies and activation volumes, as suggested by Zhang *et al.*,[28] and may be sensitive to the specific alkyl structures in the ZDDP molecules. Regardless, the large value of the activation volume for shear stress found here indicates that shear stress is very effective in driving tribofilm formation, while compressive stress is only modestly effective at inhibiting it.

There are multiple possible hypotheses for why compressive stress inhibits tribofilm formation. First, the increased compressive stress forces atoms to be closer to each other, which, on the one hand, can inhibit the bond stretching needed to assist with bond-breaking chemical reactions, while, on the other hand, it can promote bond-formation reactions by confinement (keeping reactants in close proximity) and strain (modifying the energy landscape in a way that promotes bond formation).

Second, compression may inhibit the bond-breaking reactions needed to instigate adsorption of ZDDP precursor molecules on the sliding surface. Such adsorption is critical as the first step for ZDDP-derived tribofilm formation. Yamaguchi *et al.* showed that ZDDP initially adsorbed on the substrate through the sulfur atom of the P=S bond by inelastic electron tunneling spectroscopy (IETS).[48] This agrees with a later study by Ivanov *et al.*, who investigated the formation of covalent linkages between the dithiophosphate groups and the substrate using ^{31}P proton nuclear magnetic resonance (NMR) spectroscopy.[49] This is significant as such linkages are likely to be an important prerequisite to initiate tribofilm growth. Therefore, with shear stress, the S–Zn bonds can be easily stretched or broken, which can promote the oxidation and reduction reactions between the ZDDP molecule and the sliding surface to form the tribofilm. Compressive stress likely inhibits breaking of the S–Zn bonds, which slows down the adsorption process, and thus the tribofilm growth is inhibited.

Third, compression may inhibit a key step identified in phosphate formation from ZDDP precursors. Jones *et al.* showed that the exchange between oxygen and sulfur atoms (O/S exchange) followed by the bond breakage between the sulfur atom and the alkyl group is a well-known property of organic thiophosphates.[50] Since the growth rate of secondary alkyl ZDDP-derived tribofilms is much faster than other types of ZDDPs, the rupture of the O/S–R bonds could be the rate-determining step of tribofilm formation.[28] After the adsorption of the precursor molecules, the bond cleavage of O/S–R is more likely caused by shear stress instead of compressive stress, thus the tribofilm formation rate reduces when the compressive stress is increased.

Fourth, when the surface is subjected to high compressive stress, the pressure–viscosity effect will result in a dramatically-higher-viscosity fluid within the contact.[51] Compressive stress enhances intermolecular forces, which will enhance viscosity, and, furthermore, can affect the conformation of the lubricant molecules, changing the lubricant's viscous behavior locally.[52,53] This higher viscosity will lead to lower molecular mobility, and a change to a first-order system according to the Stokes–Einstein equation:

$$D = \frac{k_B T}{6\pi r \eta} \tag{6}$$

where D is the Brownian diffusivity, and r is the radius of the molecule. Thus, the diffusivity varies inversely with the viscosity. Therefore, with the pressure-induced high local viscosity, the mobility of the ZDDP is reduced, which may constrain its ability to adsorb on the surface. Thus, the reaction rate is reduced.

As mentioned above, mechanisms by which compression should promote tribofilm growth have been identified, namely compression-induced cross-linking of the phosphate network,[30–33] and compression-induced reactions with the substrate.[34] The present results do not rule out that these mechanisms occur and are consequential for tribofilm growth and properties. However, the results do strongly indicate that such mechanisms are not rate-limiting steps that control the tribofilm growth rate; rather, a bond-breaking mechanism, inhibited by compression and promoted by shear, is the controlling reaction.

4. Conclusions

We developed a stress-controlled mechanochemical reactor, which enabled study of the independent effects of compressive stress, shear stress, and temperature on the mechanochemically-driven growth of tribofilms. The methodology incorporated the novel approach of Zhang and Spikes,[12] where MTM experiments used a combination of high- and low-traction fluids, resulting in growth experiments under fully EHL conditions where no direct solid–solid contact occurs. Thus, all growth occurred due to forces solely transmitted through the lubricant film for which the contact conditions and stresses are well-characterized, avoiding convoluting effects from other factors, such as substrate, asperity contact, and changes in applied stresses as the tribofilm grows. Our adaptation was to vary the fluid composition for each experiment so that one stress component (either shear or compression) can be held constant while the other is varied; or both held constant as the temperature is varied. The methodology was applied to a pure secondary ZDDP dissolved in the fluid blends, from which the following results were obtained:

1. The extended Eyring model,[47] a SATA-based approach, describes the growth behavior of ZDDP-derived tribofilms well. We find an activation barrier of $\Delta U_{\text{act}} = 0.54 \pm 0.04$ eV, an activation volume for shear stress of $\Delta V_{\text{act}} = 0.18 \pm 0.06\ \text{nm}^3$, and an activation volume for compressive stress of $\Delta \Omega_{\text{act}} = 0.010 \pm 0.004\ \text{nm}^3$.

2. The positive activation volumes for both shear stress and compressive stress indicate that a bond-breaking reaction is the driving force for ZDDP-tribofilm formation, instead of bond formation.

3. The reduction in ZDDP-derived tribofilm growth with increased compressive stress, while a mild effect (the activation volume is 18 times smaller in magnitude

than that for shear stress), indicates that the rate-limiting step in the series of reactions involved is one related to bond breaking, not bond formation or some other compressive-stress driven process.

4. Temperature and shear stress are each found independently to be strong factors driving ZDDP-derived tribofilm growth in accordance with prior work, but here demonstrated in the case of constant compressive stress.

5. The calculated activation energies from our work compare well with previous studies using ferrous surfaces, indicating similar reaction mechanisms.

6. The absence of wear in this study shows that cation exchange of the Zn with substrate ions, as proposed in the HSAB growth model,[30–33] is not required for tribofilm growth. Incorporation of substrate ions, notably Fe in the case of ferrous substrates, is well-documented[54,55] and certainly affects tribofilm initiation, growth, and properties. It is thus important to consider for understanding ZDDP growth on ferrous substrates and other substrate materials that can participate in cation-exchange reactions. However, the results here add to the body of work showing that ZDDP can form solid, surface-bound tribofilms with self-limited growth driven by stress-augmented thermal activation, in the absence of any cation exchange.

The ability to study different compositions of high-viscosity, high-traction fluids in the EHL regime provides unique insights, particularly the separation of normal and shear stress contributions to film growth. This enables a better understanding of the mechanochemical reactions for ZDDP-derived tribofilm formation. This approach can be beneficial for investigating the mechanisms of other reactive, film-forming additives for next-generation lubricant development.

Conflicts of interest

There are no conflicts to declare.

Acknowledgements

R. W. C. and L. F. acknowledge support from NSF grants CMMI-1728360 and CHE-2023644. We thank A. R. Konicek, D. Eichelsdoerfer, B. Gooding, A. Jaishankar, N. N. Gosvami, H, Khare, and A. Schilowitz for useful discussions. We thank J. Ford for assistance with the ToF-SIMS measurements. This work was carried out in part at the Singh Center for Nanotechnology, which is supported by the NSF National Nanotechnology Coordinated Infrastructure Program under grant NNCI-2025608.

References

1 P. A. Asseff, Lubricant, US Pat., 2,261,047, 1941.
2 J. B. Bidwell and P. Vermaire, Lifters and Lubricants, *SAE Trans.*, 1955, **63**, 211–226.
3 H. Spikes, The History and Mechanisms of ZDDP, *Tribol. Lett.*, 2004, **17**(3), 469–489.
4 G. W. Stachowiak and A. W. Batchelor, Elastohydrodynamic Lubrication, in: *Engineering Tribology*, Elsevier, 2014, pp. 293–370.

5 N. N. Gosvami, J. A. Bares, F. Mangolini, A. R. Konicek, D. G. Yablon and R. W. Carpick, Mechanisms of antiwear tribofilm growth revealed *in situ* by single-asperity sliding contacts, *Science*, 2015, **348**(6230), 102–106.

6 F. T. Barcroft, R. J. Bird, J. F. Hutton and D. Park, The mechanism of action of zinc thiophosphates as extreme pressure agents, *Wear*, 1982, **77**(3), 355–384.

7 M. L. Suominen Fuller, K. L. De Jong, M. Kasrai and G. M. Bancroft, Electroless Generation of Phosphate Films on Metals from Zinc Dialkyldithiophosphates, *Chem. Mater.*, 2000, **12**(5), 1300–1304.

8 Y. Shimizu and H. A. Spikes, The Influence of Aluminium–Silicon Alloy on ZDDP Tribofilm Formation on the Counter-Surface, *Tribol. Lett.*, 2017, **65**(4), 137.

9 N. N. Gosvami, I. Lahouij, J. Ma and R. W. Carpick, Nanoscale *in situ* study of ZDDP tribofilm growth at aluminum-based interfaces using atomic force microscopy, *Tribol. Int.*, 2020, **143**, 106075.

10 T. Haque, A. Morina, A. Neville, R. Kapadia and S. Arrowsmith, Non-ferrous coating/lubricant interactions in tribological contacts: Assessment of tribofilms, *Tribol. Int.*, 2007, **40**(10–12), 1603–1612.

11 M. Ueda, A. Kadiric and H. Spikes, ZDDP Tribofilm Formation on Non-Ferrous Surfaces, *Tribology Online*, 2020, **15**(5), 318–331.

12 J. Zhang and H. Spikes, On the Mechanism of ZDDP Antiwear Film Formation, *Tribol. Lett.*, 2016, **63**(2), 24.

13 B. Vengudusamy, J. H. Green, G. D. Lamb and H. A. Spikes, Durability of ZDDP Tribofilms Formed in DLC/DLC Contacts, *Tribol. Lett.*, 2013, **51**(3), 469–478.

14 B. Vengudusamy, J. H. Green, G. D. Lamb and H. A. Spikes, Tribological properties of tribofilms formed from ZDDP in DLC/DLC and DLC/steel contacts, *Tribol. Int.*, 2011, **44**(2), 165–174.

15 J. S. Sheasby, T. A. Caughlin and J. J. Habeeb, Observation of the antiwear activity of zinc dialkyldithiophosphate additives, *Wear*, 1991, **150**(1–2), 247–257.

16 R. J. Bird and G. D. Galvin, The application of photoelectron spectroscopy to the study of e. p. films on lubricated surfaces, *Wear*, 1976, **37**(1), 143–167.

17 J. C. Bell, K. M. Delargy and A. M. Seeney, Paper IX (ii) The Removal of Substrate Material through Thick Zinc Dithiophosphate Anti-Wear Films, *Tribol. Ser.*, 1992, **21**, 387–396.

18 J. M. Georges, J. M. Martin, T. Mathia, Ph Kapsa, G. Meille and H. Montes, Mechanism of boundary lubrication with zinc dithiophosphate, *Wear*, 1979, **53**(1), 9–34.

19 API Engine Oil Classifications, *Service Fill Oils for Gasoline, Light-Duty Diesel And Heavy-Duty Diesel Engines [Internet]. Infineum*, 2020, **https://www.infineum.com/media/w5kpot0y/api-engine-oil-classifications-brochure2.pdf**.

20 J. V. Rensselar, Special report: The tribology of electric vehicles, *Tribol. Lubr. Technol.*, 2019, **75**(34), 35–43.

21 Y. Chen, S. Jha, A. Raut, W. Zhang and H. Liang, Performance Characteristics of Lubricants in Electric and Hybrid Vehicles: A Review of Current and Future Needs, *Front. Mech. Eng.*, 2020, **6**, 571464.

22 H. S. Khare, I. Lahouij, A. Jackson, G. Feng, Z. Chen, G. D. Cooper, *et al.*, Nanoscale Generation of Robust Solid Films from Liquid-Dispersed Nanoparticles *via in Situ* Atomic Force Microscopy: Growth Kinetics and

Nanomechanical Properties, *ACS Appl. Mater. Interfaces*, 2018, **10**(46), 40335–40347.

23 M. B. Elinski, P. LaMascus, L. Zheng, A. Jackson, R. J. Wiacek and R. W. Carpick, Cooperativity Between Zirconium Dioxide Nanoparticles and Extreme Pressure Additives in Forming Protective Tribofilms: Toward Enabling Low Viscosity Lubricants, *Tribol. Lett.*, 2020, **68**(4), 107.

24 I. Lahouij, B. Gould, N. Demas, A. Greco, Z. Chen, G. D. Cooper, *et al.*, Inhibition of Micro-pitting by Tribofilm-Forming ZrO2 Nanocrystal Lubricant Additives: A Micro-pitting Rig and Transmission Electron Microscope Study, *Tribol. Lett.*, 2022, **70**(1), 13.

25 H. Kato and K. Komai, Tribofilm formation and mild wear by tribo-sintering of nanometer-sized oxide particles on rubbing steel surfaces, *Wear*, 2007, **262**(1–2), 36–41.

26 A. Dorgham, P. Parsaeian, A. Azam, C. Wang, A. Morina and A. Neville, Single-asperity study of the reaction kinetics of P-based triboreactive films, *Tribol. Int.*, 2019, **133**, 288–296.

27 N. N. Gosvami, J. Ma and R. W. Carpick, An *In Situ* Method for Simultaneous Friction Measurements and Imaging of Interfacial Tribochemical Film Growth in Lubricated Contacts, *Tribol. Lett.*, 2018, **66**(4), 154.

28 J. Zhang, J. P. Ewen, M. Ueda, J. S. S. Wong and H. A. Spikes, Mechanochemistry of Zinc Dialkyldithiophosphate on Steel Surfaces under Elastohydrodynamic Lubrication Conditions, *ACS Appl. Mater. Interfaces*, 2020, **12**(5), 6662–6676.

29 H. Spikes, Stress-augmented thermal activation: Tribology feels the force, *Friction*, 2018, **6**(1), 1–31.

30 N. J. Mosey, T. K. Woo and M. H. Müser, Mechanism of wear inhibition by ZDDP lubricant additives - Insights from molecular scale simulations, *J. Am. Chem. Soc.*, 2005, **4**, 332–335.

31 N. J. Mosey, Molecular Mechanisms for the Functionality of Lubricant Additives, *Science*, 2005, **307**(5715), 1612–1615.

32 N. J. Mosey, T. K. Woo, M. Kasrai, P. R. Norton, G. M. Bancroft and M. H. Müser, Interpretation of experiments on ZDDP anti-wear films through pressure-induced cross-linking, *Tribol. Lett.*, 2006, **24**(2), 105–114.

33 N. J. Mosey, T. K. Woo and M. H. Müser, Energy dissipation *via* quantum chemical hysteresis during high-pressure compression: A first-principles molecular dynamics study of phosphates, *Phys. Rev. B: Condens. Matter Mater. Phys.*, 2005, **72**(5), 054124.

34 M. C. Righi, S. Loehlé, M. I. De Barros Bouchet, S. Mambingo-Doumbe and J. M. Martin, A comparative study on the functionality of S- and P-based lubricant additives by combined first principles and experimental analysis, *RSC Adv.*, 2016, **6**(53), 47753–47760.

35 S. Bec, A. Tonck, J. M. Georges, R. C. Coy, J. C. Bell and G. W. Roper, Relationship between mechanical properties and structures of zinc dithiophosphate anti–wear films, *Proc. R. Soc. London, Ser. A*, 1999, **455**, 4181–4203.

36 J. M. Martin, Antiwear mechanisms of zinc dithiophosphate: a chemical hardness approach, *Tribol. Lett.*, 1999, **6**, 1–8.

37 J. Dawczyk, N. Morgan, J. Russo and H. Spikes, Film Thickness and Friction of ZDDP Tribofilms, *Tribol. Lett.*, 2019, **67**(2), 34.

38 F. A. Stevie, L. Sedlacek, P. Babor, J. Jiruse, E. Principe and K. Klosova, FIB-SIMS quantification using TOF-SIMS with Arand Xe plasma sources, *Surf. Interface Anal.*, 2014, **46**, 285–287.

39 R. G. Wilson, F. A. Stevie and C. W. Magee, *Secondary Ion Mass Spectrometry: A Practical Handbook for Depth Profiling and Bulk Impurity Analysis*, Wiley-Interscience, New York, 1st edn, 1989, p. 384.

40 P. A. Willermet, R. O. Carter and E. N. Boulos, Lubricant-derived tribochemical films—An infra-red spectroscopic study, *Tribol. Int.*, 1992, **25**(6), 371–380.

41 J. C. Bell, R. C. Coy and H. A. Spikes, Cryogenic Studies of Zinc Dialkyl Dithiophosphate Anti-wear Films, *Proc. JSLE Int. Tribol. Conf.*, 1990, **505**, 505–510.

42 J. C. Bell and K. M. Delargy, The composition and structure of model zinc dialkyldithiophosphate antiwear films, *Proceeding of the 6th International Congress on Tribology*, 1993, **2**, 328–332.

43 C. Minfray, J. M. Martin, M. I. D. Barros, T. L. Mogne, R. Kersting and B. Hagenhoff, Chemistry of ZDDP Tribofilm by ToF-SIMS, *Tribol. Lett.*, 2004, **17**(3), 351–357.

44 G. Bell, Models for the specific adhesion of cells to cells, *Science*, 1978, **200**(4342), 618–627.

45 E. Lomakina and R. E. Waugh, Bond formation during cell compression, in *Principles of Cellular Engineering*, Elsevier, 2006, pp. 105–22.

46 B. Chen, R. Hoffmann and R. Cammi, The Effect of Pressure on Organic Reactions in Fluids—a New Theoretical Perspective, *Angew. Chem., Int. Ed.*, 2017, **56**(37), 11126–11142.

47 I. M. Ward, Review: The yield behaviour of polymers, *J. Mater. Sci.*, 1971, **6**(11), 1397–1417.

48 E. S. Yamaguchi, P. R. Ryason and E. Q. Labrador, Inelastic Electron Tunneling Spectra of Neutral and Basic Zinc Dithiophosphates on Native Aluminum Oxide Surfaces, *Tribol. Trans.*, 1995, **38**(2), 243–252.

49 A. V. Ivanov, O. N. Antzutkin, A. C. Larsson, M. Kritikos and W. Forsling, Polycrystalline and surface O,O′-dialkyldithiophosphate zinc(II) complexes: preparation, 31P CP/MAS NMR and single-crystal X-ray diffraction studies, *Inorg. Chim. Acta*, 2001, **315**(1), 26–35.

50 R. B. Jones and R. C. Coy, The Chemistry of the Thermal Degradation of Zinc Dialkyldithiophosphate Additives, *ASLE Trans.*, 1981, **24**, 91–97.

51 G. W. Stachowiak and A. W. Batchelor, Physical Properties of Lubricants, in *Engineering Tribology*. Elsevier, 2014, pp. 11–50.

52 C. Barus, Isothermals, isopiestics and isometrics relative to viscosity, *Am. J. Sci.*, 1893, **s3–45**(266), 87.

53 S. Bair, The unresolved definition of the pressure-viscosity coefficient, *Sci. Rep.*, 2022, **12**(1), 3422.

54 J. M. Martin, C. Grossiord, T. L. Mogne, S. Bec and A. Tonck, The two-layer structure of Zndtp tribofilms Part I: AES, XPS and XANES analyses, *Tribol. Int.*, 2001, **8**, 523–530.

55 J. M. Martin, T. Onodera, C. Minfray, F. Dassenoy and A. Miyamoto, The origin of anti-wear chemistry of ZDDP, *Faraday Discuss.*, 2012, **156**, 311.

1. Materials

The kinematic viscosity of each fluid was measured at 40°C and 100°C using a Houillon Viscometer and the densities were obtained using the ASTM D4052 method (1). The resulting calculated dynamic viscosity at both 40°C and 100°C of each blend are shown in ***Table S1***.

#	Sample Label	$\eta_{40°C}$ (cP)	$\eta_{100°C}$ (cP)
1	99 wt% PIB + 1 wt% ZDDP	906	46
2	89 wt% PIB + 10 wt% PAO + 1 wt% ZDDP	802	43
3	84 wt% PIB + 15 wt% PAO + 1 wt% ZDDP	734	41
4	79 wt% PIB + 20 wt% PAO + 1 wt% ZDDP	675	40
5	74 wt% PIB + 25 wt% PAO + 1 wt% ZDDP	623	39
6	69 wt% PIB + 30 wt% PAO + 1 wt% ZDDP	580	38
7	64 wt% PIB + 35 wt% PAO + 1 wt% ZDDP	550	37
8	59 wt% PIB + 40 wt% PAO + 1 wt% ZDDP	512	36
9	54 wt% PIB + 45 wt% PAO + 1 wt% ZDDP	482	35

Table S1. Summary of estimated dynamic viscosity of each blend at 40°C and 100°C

2. Test methods

2.1 MTM experiment

The PCS Instruments MTM-SLIM™ (London, UK) generates both traction data and *in-situ* tribofilm thickness measurements (***Figure S1***). Each test used 15 mL of lubricant in the MTM reservoir. The ball was loaded against the disk under a preset load for a fixed duration, and both were driven independently allowing different combinations of rolling and sliding speeds. The rotations were stopped at predetermined time intervals, whereupon the ball was loaded against the spacer layer-coated window. The SLIM camera then measured the tribofilm thickness, storing an interference image for post-processing. The measurement location on the ball was the same throughout the test. The SLIM methodology is described elsewhere (2). We also measured the final end-of-test film profile using aTencor™ P-7 (Milpitas, CA) 2-D surface profilometer to verify the accuracy of the SLIM measurements.

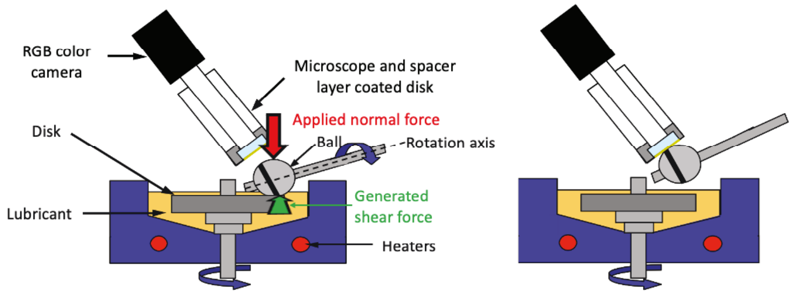

(a) (b)

Figure S1. Schematic diagram of the MTM-SLIM setup (adapted from PCS Instruments' MTM-SLIM user manual): (a) To generate the tribofilm, the ball is loaded against the disk, and run with a preset load and slide-to-roll ratio.

Different shear forces are generated depending on the applied load, fluid type and the temperature. (b) Once in a while, the test stops, and the ball is loaded against the lens of the microscope to measure the tribofilm thickness.

The maximum normal load in the MTM is 75 N, which corresponds to a maximum (mean) compressive Hertzian stress of 1.2 (0.80) GPa for standard steel balls and discs. Based on prior work, increasing the stresses beyond this limit is crucial to promote tribofilm growth within reasonable time frames (3,4). We thus used tungsten carbide (WC) balls and discs whose higher elastic modulus permits increasing the maximum Hertzian stress to 2.6 GPa (4). Note that many studies report tribofilm growth on standard steel materials in the MTM. However, these studies were conducted under mixed or boundary lubrication conditions where the maximum stresses at individual asperity contacts are much higher than the idealized Hertzian stress expected in the fluid.

The test specimens and the material properties are shown in ***Table S2***. The root-mean-square roughness of the ball and the disc was measured using a Zygo NewView™ 6300 (Middlefield, CT) white light interferometer. The measurement length is approximately 700 µm. A cut-off length of 80 µm was applied to minimize the curvature effect from the specimens (5). The values were averaged from six repeated measurements.

	WC ball	**WC disc**
Diameter	19.05 mm	46 mm
$\boldsymbol{\sigma}$	5 nm	2 nm

	WC material properties
$\boldsymbol{E}$	600 GPa
$\boldsymbol{\nu}$	0.293

Table S2. Test specimen information and material properties

Before each experiment, the specimens were sonicated in toluene and isopropanol for 15 minutes each, and dried using compressed nitrogen gas. A Kimwipe was gently wiped on the specimens to remove fibers or any other residues. After each experiment, all the MTM and SLIM components and test specimens were sonicated in toluene and isopropanol again for 15 mins. Droplets of 0.05M of ethylenediaminetetraacetic acid (EDTA) solution were applied to the film area of the test specimen for 1 minute to remove the ZDDP tribofilm (6). Then, a 15-min sonication with deionized (DI) water to remove EDTA residue. This procedure allowed for re-use of the WC specimens multiple times before visible signs of surface distress were noted.

2.2 ToF-SIMS experiment

The ToF-SIMS analysis was carried out with a xenon (Xe^+) primary ion source with 10kV energy and 10 nA of current, and with a spatial resolution of 256 x 256 pixels. A large 400 x 400 µm^2 field of view was used; this reduces the risk of unintentionally damaging the tribofilm. The method for collecting sample data is shown in ***Figure S2 (a)***. To convert the unit of depth from number of frames to thickness in nm, an approximate calibration was made. The average height of the tribofilm shown in **Figure S2(c)** was estimated to be 80 nm from the WLI measurement in ***Figure S2(b)***. After ToF-SIMS measurement milling for 8000 frames, the trench was found to be approximately 200-nm deep shown in ***Figure S2(e)*** from the WLI measurement in ***Figure S2(d)***. Therefore, the depth resolution of this study is around 0.035 nm/frame.

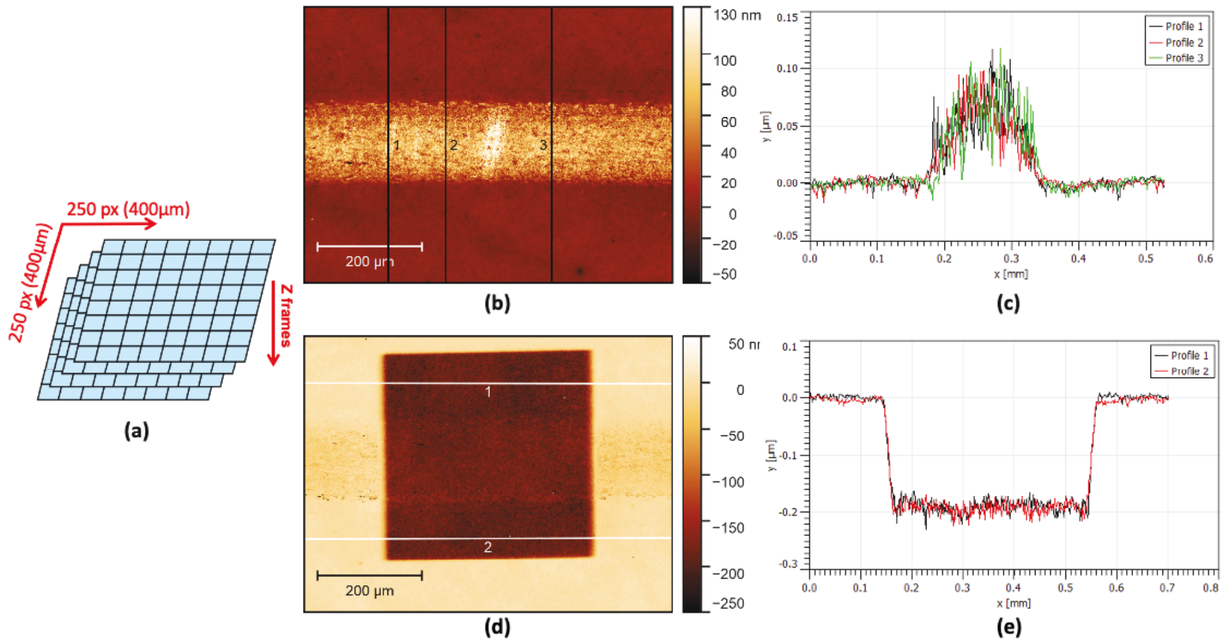

Figure S2. (a) Schematic illustration of the ToF-SIMS measurement in x, y, and z directions [adapted from Tescan manual]. (b) The WLI image of the running track on the WC disc before the ToF-SIMS experiment and (c) the corresponding average height of tribofilm, measured from 3 different line profiles. (d) The WLI image of the running track on the WC disc after 8000-frame of milling from ToF-SIMS experiment, and (e) the average height in the tribofilm area.

3. Characterizing test fluid properties

3.1 Traction Behavior

To measure the shear stress for each blend, the traction behavior of each fluid was characterized at applied loads varying between 23.5 to 68 N. This range yields Hertzian maximum contact stresses from 1.75 to 2.5 GPa as shown in ***Table S3***. For each load condition, the test temperature was varied at 20°C intervals from 20°C to 140°C.

F (N)	P_{max} (GPa)	R (µm)
23.5	1.75	80
38	2	93.9
40	2.1	95.5
46.5	2.2	100.4
49.5	2.25	102.5
53	2.3	104.9
60.5	2.4	109.6

68	2.5	114

Table S3. Summary of applied load with the corresponding idealized Hertzian stress, and contact radius.

For the traction experiments, the entrainment speed was held at 2000 mm/s and the slide-to-roll Ratio (SSR), as defined in equation (S1), was varied from 0 to 100%:

$$SRR = \frac{|U_{disc} - U_{ball}|}{U} \text{ x } 100\% \qquad \text{(S1)}$$

PIB was selected due to its high traction coefficient in EHL conditions. ***Figure S3(a)*** compares the traction response between the PIB and the PAO. Since PIB exhibits higher EHL traction than PAO, it can generate a much greater traction coefficient at any SRR. By mixing these two fluids together, it is possible to create fluids with various of traction properties. This allows us to independently control the shear stress within the contact zone at any given normal stress and temperature.

The PIB traction curve in ***Figure S3(b)*** reaches a maximum at approximately 10% SRR. The reduction in traction at higher SRR is known as the thermal EHL region, when frictional heating of the lubricant in the inlet and contact region acts to lower the effective viscosity, and hence the shear stress (7). To reduce the effect of frictional heating, all of the MTM-SLIM film-forming experiments were performed at 6% SRR. The traction response of each blend at this SRR is below the maximum traction coefficient for each test fluid but is sufficiently high to generate a ZDDP tribofilm.

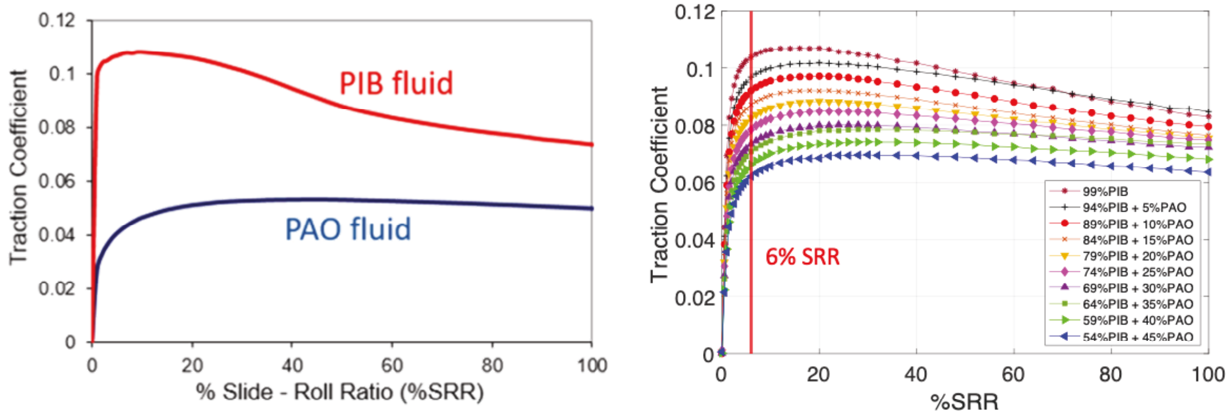

(a) (b)

Figure S3. (a) The traction curves of PIB and PAO fluids under 2.5 GPa and 100°C. (b) EHL traction coefficient as a function of SSR for different blends at 2.5 GPa and 140°C. 6% SRR was used for all tribofilm experiments to eliminate frictional heating.

The shear stress is estimated by using the maximum Hertzian stress, and the measured traction coefficient:

$$\tau_{max} = \mu_{6\%SRR} P_{max} \qquad \text{(S2)}$$

A summary of maximum shear stresses generated at 6% SRR as a function of composition at different temperatures and compressive stress is shown in ***Figure S4***. Under different conditions, it was possible to vary the shear stress between 80 MPa to 264 MPa.

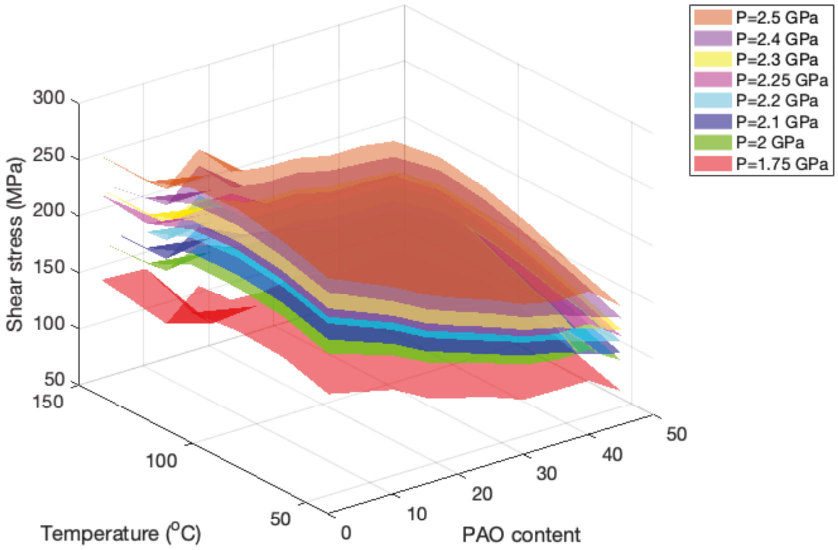

Figure S4. Maximum shear stress as a function of composition at different temperatures and pressures (6% SRR).

3.2 Specific film thickness characterization

To ensure there is no surface contact in our experiments, we used equation (S3) to calculate specific film thickness (8):

$$\lambda = \frac{h_c}{\sqrt{\sigma_{ball}^2 + \sigma_{disc}^2}} \quad \text{(S3)}$$

Typically, $\lambda > 3$ implies a full elastohydrodynamic condition in which there is no surface contact. The central film thickness, h_c, can be determined by using Cheng's equation (9) in equation (4) .

$$h_c = 1.415R_a * \left(\frac{\eta_0 \alpha U}{R_a}\right)^{0.725} * \left(\frac{P}{E_a}\right)^{-0.174} \quad \text{(S4)}$$

Where U is the entrainment speed:

$$U = \frac{1}{2}(U_{ball} + U_{disc}) \quad \text{(S5)}$$

The central film thickness of different blends was measured using the PCS instruments optical EHL apparatus. An example of EHL film thickness measurement as a function of rolling speed is shown in ***Figure S5***. From these measurements, it is possible to extract the missing lubricant-related properties in equation (4). Using the calculated lubricant properties for each blend it is possible to reapply equation (4) to the materials and operating conditions in the MTM experiments. The resulting film thickness values are then used in equation (3) to calculate the specific film thickness. The specific film thickness of all experiments is greater than 15, which corresponds to the case of 54 wt% PIB + 45 wt% PAO blend at 140°C and 2.5 GPa. This shows that there is a high degree of separation between the surfaces.

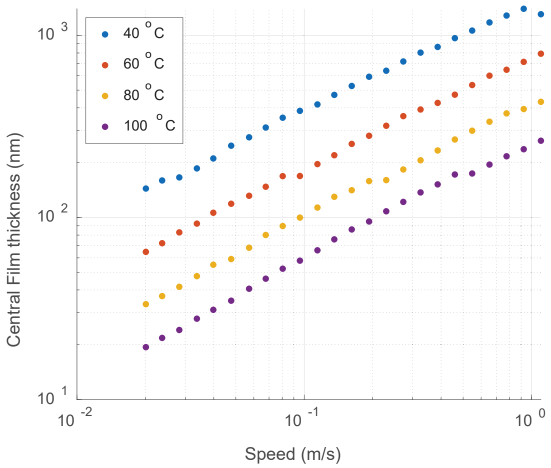

Figure S5. EHL film thickness of 64%PIB + 35% PAO in pure rolling.

3.3 Tribofilm thickness measurement

An example of a SLIM image is shown in ***Figure S6***. The image resolution is 0.7 μm per pixel. The film thickness at each pixel is extracted using the combination of the refractive index of the lens and tribofilm as listed in ***Table S4*** and the measured values from the optical measurement (10).

	Refractive index	**Reference**
MTM lens	1.4	(2)
ZDDP tribofilm	1.6	(6)

Table S4. The refractive index of MTM lens and ZDDP tribofilm.

For our calculations of average tribofilm thickness we used a circular analysis area of 144 μm in diameter. This value corresponded to the largest width of the tribofilm that was produced. After obtaining a series of SLIM images during the test, the film thickness and volumetric growth over time can be calculated.

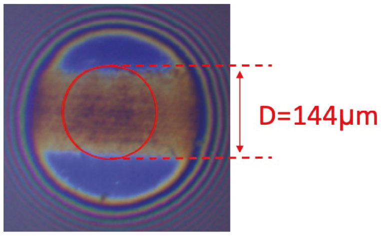

Figure S6. An example of a SLIM image of a ZDDP tribofilm.

3.4 Tribofilm Growth and Morphology

To capture the initial fast growth of the tribofilm, especially with high shear stress and temperature, the interference image was taken more frequently in the initial time interval. The frequency of different time intervals is summarized in ***Table S5***.

Time	SLIM Imaging Frequency
0—10 minutes	Every 1 minute
10—30 minutes	Every 5 minutes
30—60 minutes	Every 10 minutes
60—360 minutes	Every 30 minutes

Table S5. The frequency of SLIM images taken at different time periods.

An example of a series of SLIM images obtained with 99%PIB + 1% ZDDP from a 360-minute test is shown in ***Figure S7***. A patchy tribofilm was observed to grow initially in the middle of the contact, where both the normal and shear stress is at the maximum value. It appears that the growth extends from this region toward the edges. A possible explanation is that the Hertzian stress reduces away from the center of the contact and thus it takes longer for the film to grow in areas away from the central region. The corresponding traction coefficient in ***Figure S8*** shows that the shear stress stays almost constant during the experiment.

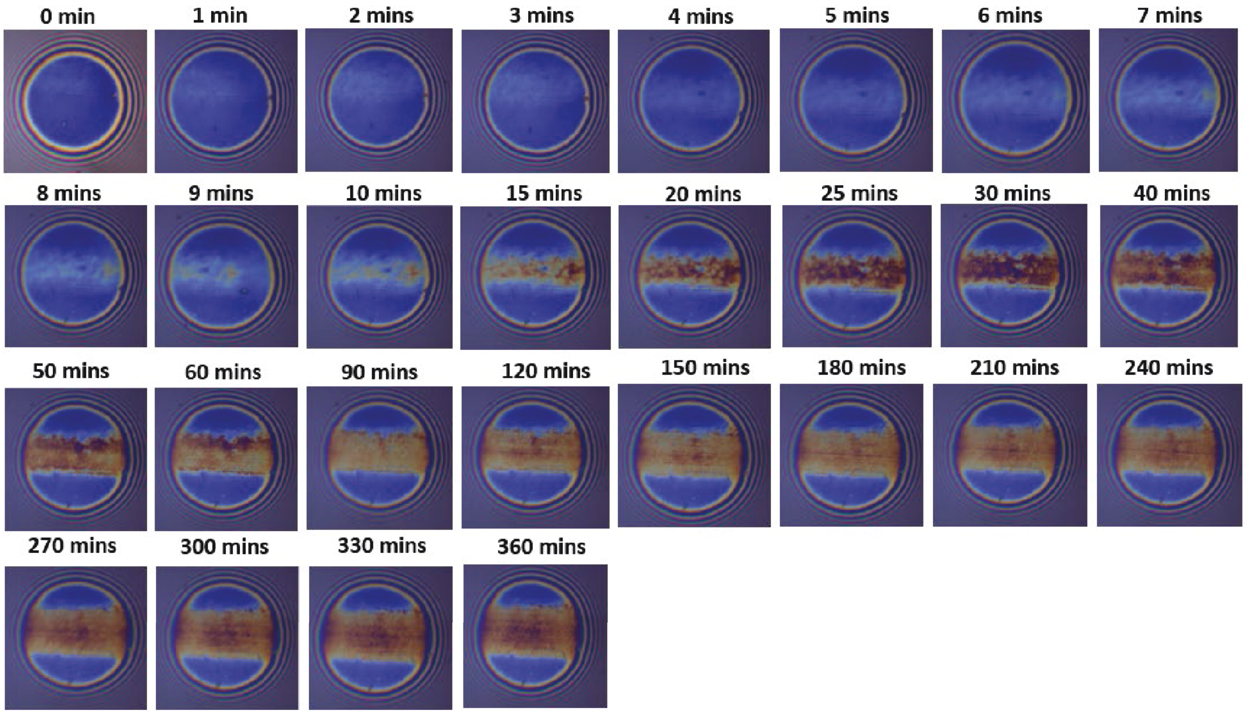

Figure S7. SLIM images of ZDDP tribofilm formation with 99%PIB + 1% ZDDP at 140°C under 2.5 GPa applied stress, which corresponds to 260 MPa shear stress.

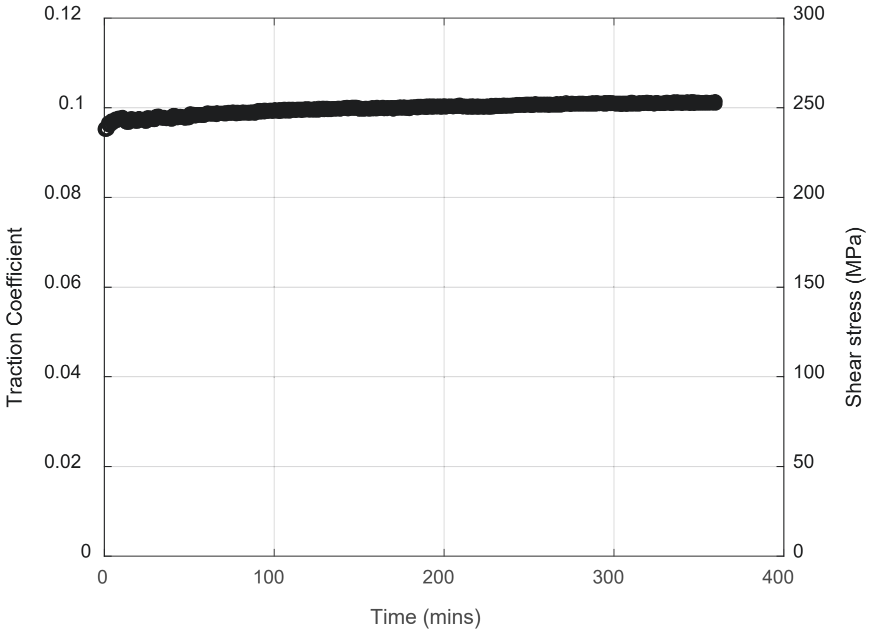

Figure S8. The traction coefficient (the shear stress) is stable over time with 99%PIB + 1% ZDDP under the compressive stress of 2.5 GPa at 140°C

Figure S9 shows the corresponding film growth dynamics based on averages calculated over the area shown in ***Figure S7***. At this shear stress (260 MPa), the tribofilm thickness rapidly reached a maximum at 30 minutes, then started to decline before continuing to grow back to approximately the same thickness. A similar effect was observed by Gosvami *et al.* in AFM-based growth experiments which have high spatial resolution of the tribofilm, and was attributed to the competition between film growth and removal (3). In our case, since direct physical contact is unlikely to have occurred during the sliding experiment, this film removal and formation could indicate that there are some inherent properties of the ZDDP tribofilm that limit the growth mechanisms. Ueda *et al.* explored the crystalline structure of ZDDP tribofilms grown in MTM under boundary lubrication conditions, where the outer region of the tribofilm is amorphous and can be easily removed, while the inner region is nanocrystalline, which is thus assumed to be much stronger and durable (11). The removal of tribofilm observed here indicates that the weaker amorphous structure of the outermost region tribofilm could not withstand the shear-induced by the fluid. After this transient period where the amorphous region is presumably removed, the formation rate modestly exceeds the removal rate, since the nanocrystalline structure in the bottom of the tribofilm cannot be removed easily.

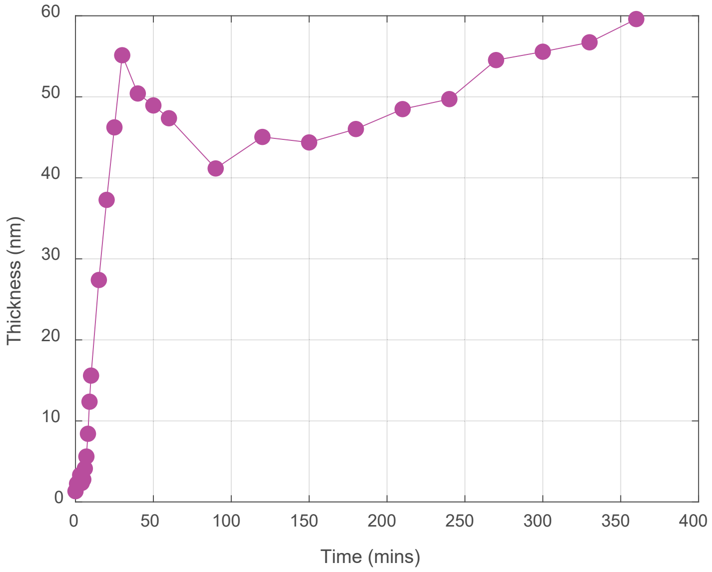

Figure S9. The evolution of the average thickness of a ZDDP tribofilm growth with 99%PIB + 1% ZDDP at 140°C under 2.5 GPa applied stress, which corresponds to 260 MPa shear stress.

In this study, we observed that the thickness reaches to a saturation at 30 minutes with higher traction fluid at higher shear stress and higher temperautre. On the other hand, there is a very thin film deposited for the first 10 minutes with lower traction fluid at low shear stress and low temperature, thus the thickness cannot be accurately measured by the SLIM system.

Therefore, the data between 10 to 30 minutes are included for the volumetric growth rate calculation, with a linear fit performed for all the experiments.

The tribofilm growth vs. time was recorded under different conditions. For the shear stress study, ***Figure S10(a)*** and ***Figure S10(c)*** show the variation of both tribofilm thickness and volume under the condition listed in experiment Subset 1 and Subset 2 respectively in ***Table 2***. As specified above, the growth rates were extracted using a linear fit from 10 to 30 minutes as shown in ***Figure S10(b)*** and ***Figure S10(d)***. Similarly, the tribofilm responses of the two experimental subsets of temperature and compressive stress are displayed in ***Figure S11*** and ***Figure S12*** respectively. The extended Eyring model fit is performed using the curve fitting function in Matlab. The error bar is the 95% confidence interval calculated by Matlab.

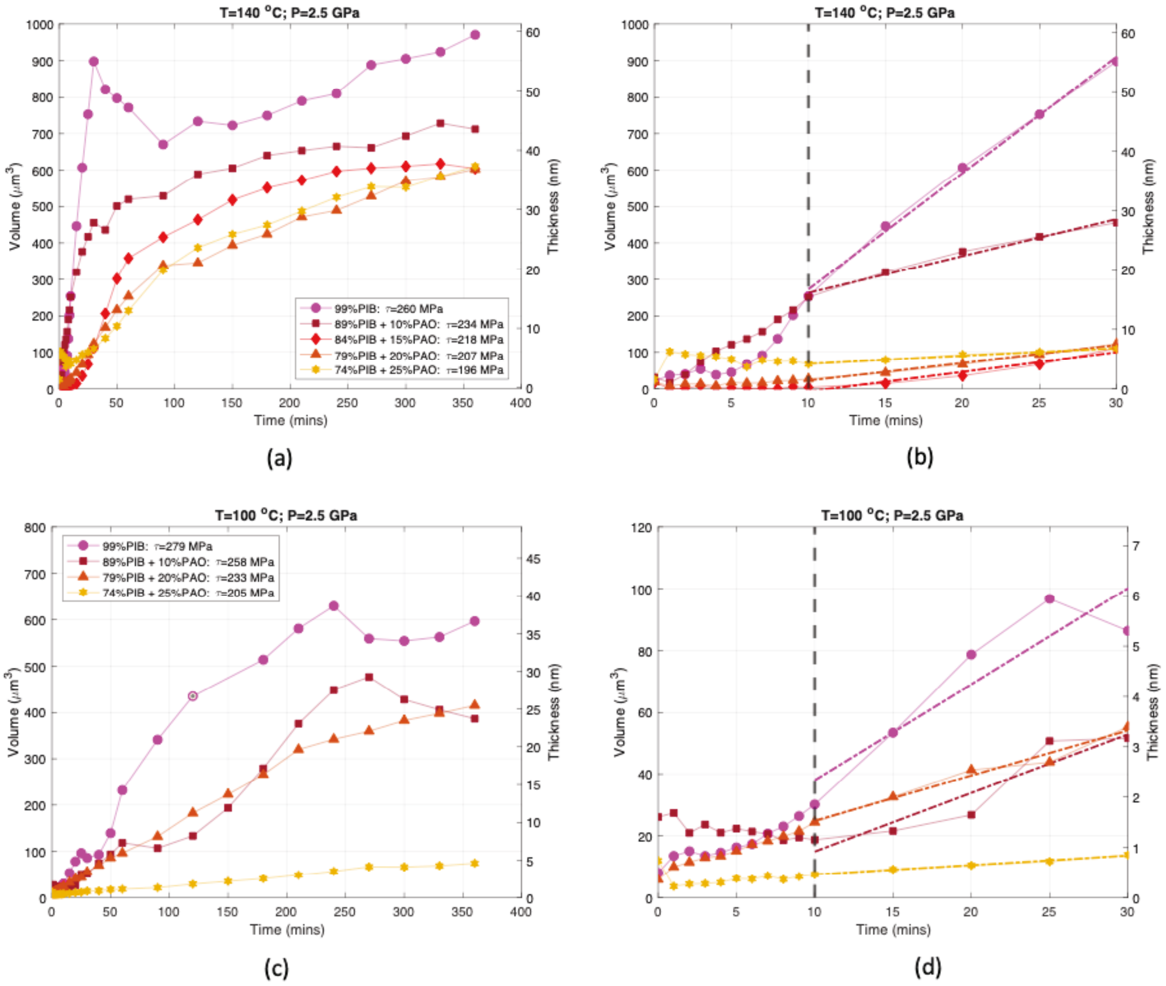

(a) (b)

(c) (d)

Figure S10. Effect of shear stress on tribofilm formation for (a) experiment Subset 1: T=140°C & P=2.5 GPa with the first 30 minutes shown in (b), and (c) experiment Subset 2: T=100°C; P=2.5 GPa with the first 30 minutes shown in (d). The growth rates were estimated from a linear fit between 10 to 30 minutes for experiment Subset 1 and experiment Subset 2 as shown in (b) and (d).

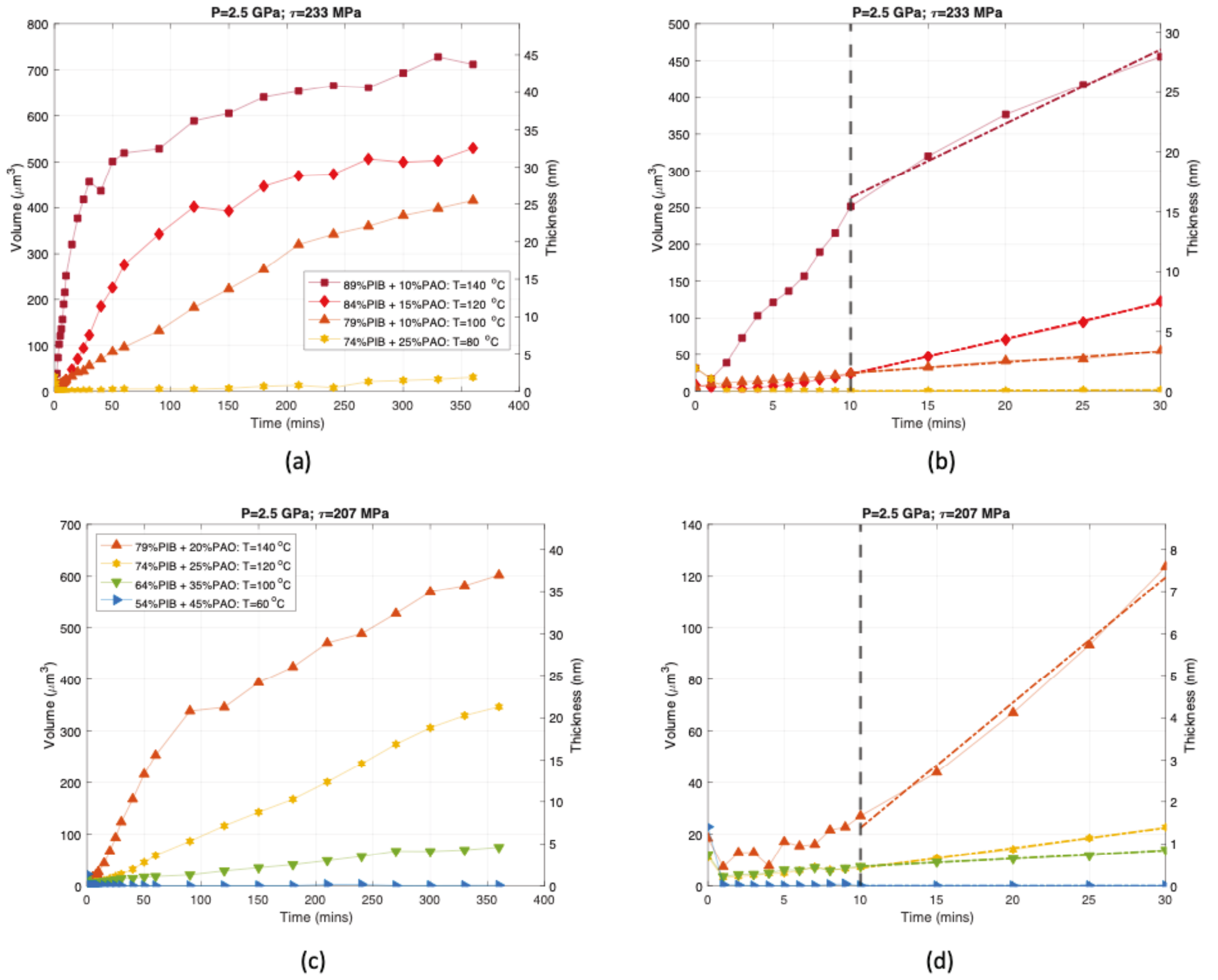

Figure S11. Effect of temperature on tribofilm formation of (a) experiment Subset 1: P=2.5 GPa; τ=233±2 MPa with the first 30 minutes shown in (b), and (c) experiment Subset 2: P=2.5 GPa; τ=207±2 MPa with the first 30 minutes shown in (d). The growth rates were estimated from a linear fit between 10 to 30 minutes for experiment Subset 1 and experiment Subset 2 as shown in (b) and (d).

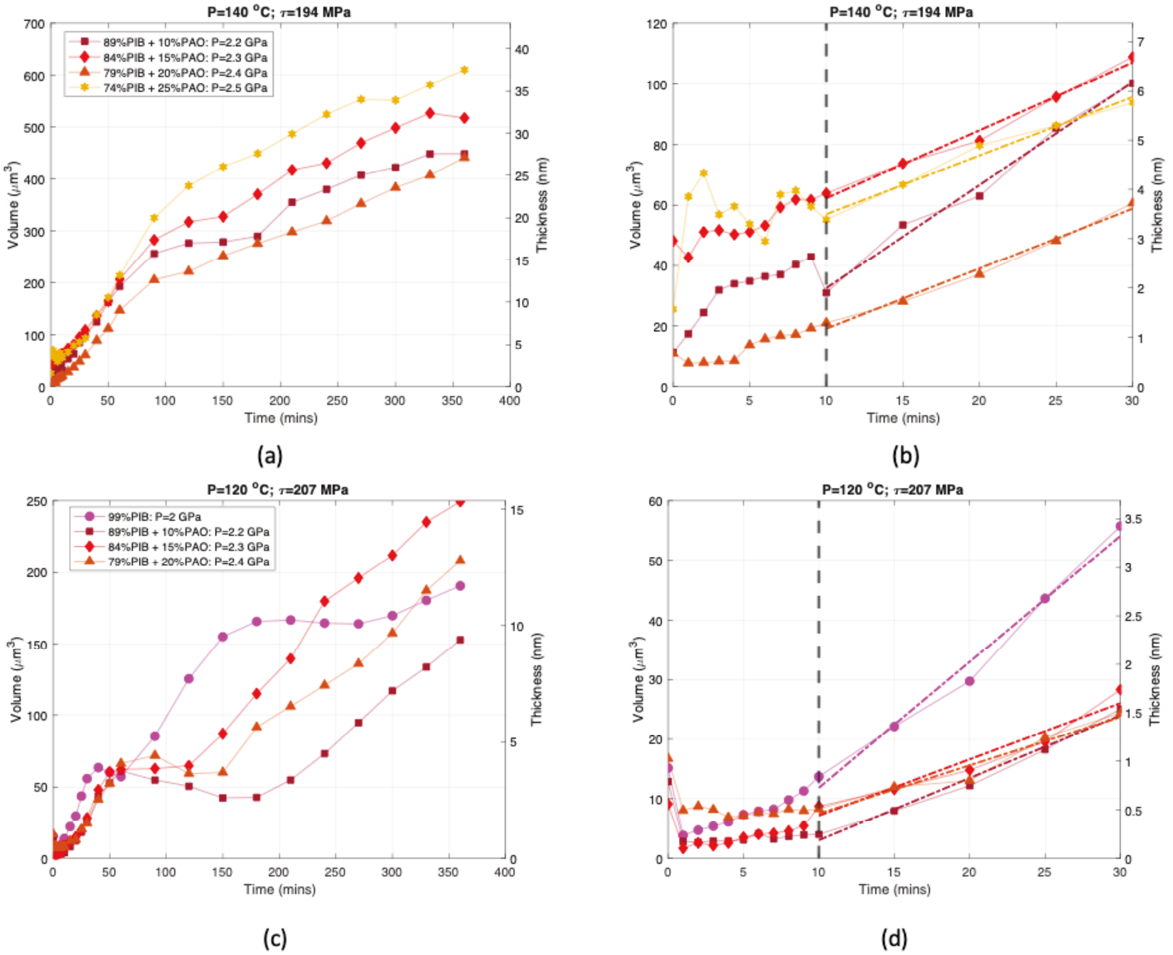

(a) (b)

(c) (d)

Figure S12. Effect of compressive stress on tribofilm formation of (a) experiment Subset 1: T=140°C; τ=194±2 MPa with the first 30 minutes shown in (b), and (c) experiment Subset 2: T=120°C; τ=207±2 MPa with the first 30 minutes shown in (d). The growth rates were estimated from a linear fit between 10 to 30 minutes for experiment Subset 1 and experiment Subset 2 as shown in (b) and (d).

Note that this study uses the maximum compressive stress and maximum shear stress values for fitting the extended Eyring model to determine the activation energy and volume for each data set. Based on the Hertizan stress model, the mean stress is 2/3 of the maximum stress. If the mean compressive stress and shear stress were used in the extended Eyring model fit, and using $\Delta U_{act} = 0.54\ eV$ from Table 4, $\Delta V_{act} = 0.27\ nm^3$ and $\Delta\Omega_{act} = 0.0132\ nm^3$ were obtained. Those values are approximately 3/2 of the values shown in Table 4 as expected. We note that some literature papers use the mean stress instead of the maximum stress and so care should be taken in comparing values between different publications. This lack of standardization is a concern, but we believe an even more significant issue is the fact that the stress values are in fact not constant throughout the contact. This will be addressed in a future publication.

Since the fluid viscosities of our oils are high, sometimes during the SLIM measurement the oil will get trapped at the center of the contact when the ball is initially put in contact with the SLIM window, particularly when the test temperature is low. ***Figure S13*** shows an example of oil trapped at the center of the contact. When analyzing the tribofilm thickness, we avoided the oil pocket area. Despite this, the oil pocket is sometimes too large in the beginning period of some of our tests, especially the first 10 mins, and it was not possible to avoid having the oil pocket be within the pre-defined SLIM analysis area for determining film thickness. Therefore, the oil pocket sometimes leads to a misleadingly high film thickness in early tribofilm thickness measurements. This can be seen, for example, in ***Figure S10(d)*** for the 89%PIB + 10% PAO data set. This artifact diminished after the initial 10 minutes due to the formation of tribofilm on the surface. One way to reduce the effect is to increase the hold time between the ball and the microscope when doing the SLIM imaging. This allows the trapped oil to leak away. However, that would add significant time to the experiment, and was not performed so that all the experiments could be conducted with the same timing

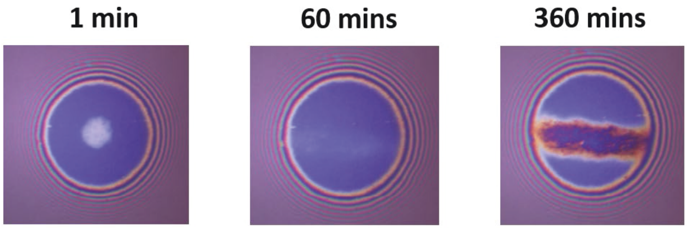

Figure S13. An example of oil trapped at the center of the contact for 89%PIB+10%PAO under 2.5 GPa at 100˚C

4. Nomenclature

E	Young's modulus
E_a	Reduced Young's modulus
F	Applied load
h_c	EHL central film thickness
P_{max}	Maximum Hertzian pressure
R	Contact radius
R_a	Reduced radius
SRR	Slide-to-roll ratio
U	Entrainment speed
U_{ball}	MTM ball speed
U_{disc}	MTM disc speed

α	Pressure-viscosity coefficient
η	Dynamic viscosity
η_0	Dynamic viscosity at atmospheric pressure
λ	Specific film thickness
μ	Traction coefficient
ν	Poisson's ratio
σ	RMS roughness
τ_{max}	Maximum shear stress

5. Reference

1. D02 Committee. Test Method for Density, Relative Density, and API Gravity of Liquids by Digital Density Meter [Internet]. ASTM International; [cited 2021 Jul 26]. Available from: http://www.astm.org/cgi-bin/resolver.cgi?D4052-18A

2. Spikes HA, Cann PM. The development and application of the spacer layer imaging method for measuring lubricant film thickness. Proc Inst Mech Eng Part J J Eng Tribol. 2001 Mar 1;215(3):261–77.

3. Gosvami NN, Bares JA, Mangolini F, Konicek AR, Yablon DG, Carpick RW. Mechanisms of antiwear tribofilm growth revealed in situ by single-asperity sliding contacts. Science. 2015 Apr 3;348(6230):102–6.

4. Zhang J, Spikes H. On the Mechanism of ZDDP Antiwear Film Formation. Tribol Lett. 2016 Aug;63(2):24.

5. Kadiric A, Sayles RS, Zhou XB, Ioannides E. A Numerical Study of the Contact Mechanics and Sub-Surface Stress Effects Experienced Over a Range of Machined Surface Coatings in Rough Surface Contacts. J Tribol. 2003 Oct 1;125(4):720–30.

6. Dawczyk J, Morgan N, Russo J, Spikes H. Film Thickness and Friction of ZDDP Tribofilms. Tribol Lett. 2019 Jun;67(2):34.

7. Lafountain AR, Johnston GJ, Spikes HA. The Elastohydrodynamic Traction of Synthetic Base Oil Blends. Tribol Trans. 2001 Jan;44(4):648–56.

8. Stachowiak GW, Batchelor AW. Elastohydrodynamic Lubrication. In: Engineering Tribology. Elsevier; 2014. p. 293–370.

9. Cheng HS. A numerical solution of the elastohydrodynamic film thickness in an elliptical contact. J Tribol Technol. 1970 Jan 1;92(1):155–61.

10. Fujita H, Spikes HA. The formation of zinc dithiophosphate antiwear films. Proc Inst Mech Eng Part J J Eng Tribol. 2004 Apr;218(4):265–78.

11. Ueda M, Kadiric A, Spikes H. On the Crystallinity and Durability of ZDDP Tribofilm. Tribol Lett. 2019 Dec;67(4):123.